Interatomic force-fields for silicas, aluminophosphates, and zeolites - derivation based on abinitio calculations

Interatomic force fields for silicas, aluminophosphates, and zeolites: Derivation based on *ab initio* calculations

G. J. Kramer, N. P. Farragher, and B. W. H. van Beest
Koninklijke/Shell-Laboratorium, Amsterdam (Shell Research B.V.), P. O. Box 3003, 1003 AA Amsterdam, The Netherlands

R. A. van Santen
Laboratory of Inorganic Chemistry and Catalysis, Eindhoven University of Technology, P. O. Box 513, 5600 MB Eindhoven, The Netherlands

(Received 2 August 1990)

A consistent force field for the description of interatomic interactions within silicas, aluminophosphates, and zeolites[1] is presented. The derivation of parameters is based both on a fit to the potential-energy surface of small clusters, as determined by *ab initio* quantum-chemical methods, and on fitting of experimental data on α-quartz. It is shown that both types of data are essential for the development of an accurate and transferable force field. The accuracy and transferability of the force field is assessed by comparing force-field predictions for the structure and elastic properties of a dozen different systems with experiment. Results obtained with the present approach compare favorably with those obtained with force fields used in the literature. Moreover, the introduction of additional chemical elements into the force field does not seriously affect the accuracy, making these force fields a valuable tool for the modeling of chemically complex zeolites.

I. INTRODUCTION

The rich polymorphism of both synthetic and mineral silicas and zeolites,[1] combined with their technological importance as selective catalysts and absorbents, has induced widespread interest in the physical and chemical properties of these systems.[2] Because of the crystallographic and compositional complexity of many of these zeolites, it is often difficult to obtain enough experimental information to form a detailed picture of, for instance, the microscopic structure of a zeolite. At this point, complementary theoretical information is very useful. Again, because of the intrinsic complexity of the systems (large unit cells, low symmetry), quantum-mechanical methods cannot be applied. Therefore in the modeling of zeolites one often uses classical force fields to describe the interatomic interaction.

Although the successes obtained with force fields have been numerous, the applicability of the traditional, empirical force fields is limited. Empirical parametrization of force fields is done by optimizing the correspondence between calculated and measured properties of simple systems such as α-quartz. As a consequence, the parametrization depends heavily on the system chosen. Transferability to other systems is questionable since no microscopic information of, e.g., the silicon oxygen bond has been used. Furthermore, this approach is limited to the description of relatively simple systems (e.g., SiO_2) since for more intricate systems ($AlPO_4$) the number of parameters exceeds the number of truly independent experimental observables. Therefore modeling of new and interesting systems, such as silica-aluminophosphates (SAPO's, $Si_{1-x-y}Al_xP_yO_2Na_{x-y}$), is impossible.

To overcome these problems and limitations, it is advantageous to base the force fields on microscopic information of the silicon oxygen bond (or Al—O, P—O, etc.), rather than on macroscopic information, such as crystal structure, elasticity, or vibrational spectrum. Such microscopic information can be obtained from the potential-energy surface of small representative clusters that can be calculated by quantum-chemical methods. In recent years, this approach has been used by various authors.[3–5] Recently, we showed in Ref. 6 that microscopic information alone does not suffice to produce a reliable force field for the simulation of infinite lattices.

This paper describes in more detail the procedure of force-field derivation, outlined in Ref. 6, and gives a complete account of the validation of the resulting force field by comparing its predictions for various silica and aluminophosphate polymorphs with experiment. Furthermore, the results are supplemented with a check on the sensitivity with respect to changes in the potential-energy surface and with extensions to the nonframework elements sodium and chlorine, enabling the modeling of zeolites of complex composition.

The outline of the paper is as follows. In Sec. II we present details of the quantum-chemical methods and clusters that were used for the construction of a potential-energy surface that contains information on the stretching and bending of the chemical bonds concerned. The functional form of the force field and its parametrization on the basis of microscopic information is discussed in Sec. III. It appears essential to include bulk information into the parametrization (Sec. IV), since otherwise a feature as simple as the crystal symmetry of quartz is wrongly predicted (Sec. IV A). The optimum force field is obtained by fitting parameters alternatingly to the potential-energy surface and to bulk information. The resulting force field is presented in Sec. IV B. In the subsequent section (Sec. V), the force-field predictions for the structure and elasticity of several SiO_2 and $AlPO_4$

polymorphs are compared both with experiment and (for SiO_2) with other force-field predictions. The statistical accuracy of *ab initio* based force fields is much better than that of empirical force fields. Also, the quality of the predictions does not deteriorate as the systems under consideration become more complicated, i.e., contain more atomic species. In Sec. VI the calculated vibrational spectrum of α-quartz is presented and a comparison with experiment is made. It appears that the difference between the experimental and the computed spectrum of α-quartz can be related to the accuracy of the cluster calculations. Finally, in Sec. VII, the extension of the force field to include nonframework elements is discussed. This is essential for the simulation of true zeolites with a negatively charged framework, compensated by cations residing in the zeolite pores and cages. Calculations on mineral sodalite ($Na_8Si_6Al_6O_{24}Cl_2$) and zeolite X ($Na_{96}Si_{96}Al_{96}O_{384}$) are presented.

II. POTENTIAL-ENERGY SURFACES OF SMALL CLUSTERS

We chose the molecular clusters H_4TO_4 (T=Si, Al, P, etc.) to represent the building blocks of zeolites. Their structure is shown in Fig. 1. Since we will parametrize its potential-energy surface and use the parametrization to describe extended systems we implicitly assume that the chemical T—O bond in this cluster is identical to the T—O bond within an extended system. In the theoretical chemical literature, this silanol molecule and the corresponding dimers, trimers, etc. have been shown to reproduce bulk properties of zeolites.[7] The fact that oxygen is sp^2 hybridized as in silcas makes this cluster, in our opinion, better suited than SiO_4^{4-} used by Tsuneyuki *et al.*[5] An additional objection to the latter cluster is the fact that the O:Si charge ratios in the cluster and in the bulk are completely different. Tsuneyuki *et al.* resolve this problem by using an *ad hoc* screening scheme to overcome this problem.

The relevant interactions within the cluster and bulk are (i) the attraction between the central atom and the surrounding oxygen atoms and (ii) the oxygen-oxygen repulsion, which stabilizes the TO_4 tetrahedron. In order to separate these interactions, we determine the potential-energy surface along two modes of distortion: the D_{2h} mode, where the oxygens are bent toward one another pairwise, and the T_d mode, being the symmetric stretching of all T—O bonds.[8] We use the optimized geometries of the TO_4 clusters as starting points of the deformations. The optimization was done at the 6-31g* restricted Hartree-Fock self-consistent-field (RHF-SCF) level using the GAMESS molecular-orbital package.[9,10] The core electrons were described with the effective core potentials of Barthelat.[11] Polarization functions were added on both the T atoms and the oxygen. The bond lengths and angles are given in Table I. Note that the difference in equilibrium bond lengths is the same as in quartz and berlinite.[12,13]

The potential-energy surface of $H_4AlO_4^-$, H_4SiO_4, and $H_4PO_4^+$ was calculated for T_d (1.35 Å $\leq r_{T\text{-}O} \leq$ 2.0 Å) and D_{2h} (70° $\leq \angle$O-T-O $\leq$ 150°) deformations using the same basis set as mentioned before. Figure 2 shows the results. The differences in T-O bonding for different T atoms are obvious from the T_d mode results. The differences in the D_{2h} mode potential-energy curves can be thought of as resulting from the size differences between the tetrahedrons.

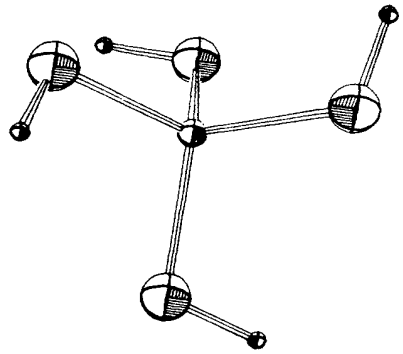

FIG. 1. H_4TO_4 cluster used for the calculation of potential-energy surfaces.

In order to test the influence of the Hartree-Fock approximation (the neglect of correlation effects) on the shape of the potential-energy surface, we have performed a few additional calculations on the H_4SiO_4 cluster. For some T-O distances along the T_d mode of distortion, we have performed both second-order Møller-Plesset (MP2) and single-double correlation-interaction (SDCI) calculations. The approximate nature of these methods implies that only part of the correlation energy (roughly half if it) is recovered in these calculations.[14] A different method for assessing the correlation energy is to use Hartree-Fock-Slater X_α-type calculations.[15] This method is a specialized case of the local-density method.[16] These methods take electron correlation effects into account through a local-density expression. Whereas it is known that the *ab initio* schemes always underestimate the correlation energy, it is difficult to assess the degree to which X_α calculations reproduce this energy. It is noted that within the field of local-density methods in general, attempts have been made to separate exchange and correlation terms (see, e.g., Ref. 17).

TABLE I. 6-31g* RHF-SCF equilibrium conformations and Mulliken populations of the H_4TO_4 clusters. Lengths are in angstroms, angles in degrees.

	$H_4AlO_4^-$	H_4SiO_4	$H_4PO_4^+$
$r(T\text{-}O(i))$	1.772	1.625	1.532
$\angle O(i)\text{-}T\text{-}O(j)$	109.47	109.47	109.47
$r(O(i)\text{-}H(j))$	0.949	0.949	0.960
$\angle H(i)\text{-}O(i)T$	113.22	119.92	125.00
$\angle H(i)\text{-}O(i)\text{-}T\text{-}O(i+1)$	0.00	0.00	0.00
q_T	1.54	1.78	2.08
q_O	−1.05	−0.93	−0.83
q_H	0.41	0.48	0.56

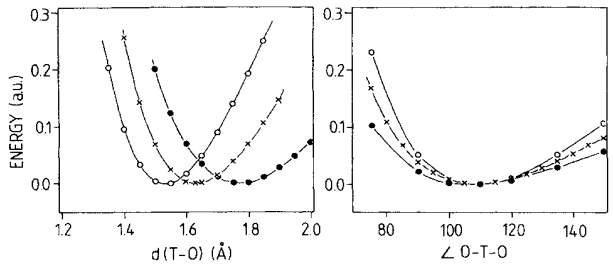

FIG. 2. Potential-energy surfaces of H_4SiO_4 (crosses), $H_4AlO_4^-$ (solid circles), and $H_4PO_4^+$ (open circles), distorted along the T_d mode (left) and along the D_{2h} mode (right). Calculations are performed at the 6-31g* RHF-SCF level.

Figure 3 shows the results of the various calculations. The minima of the curves have essentially the same locus and the difference is seen primarily with the curvature at the equilibrium bond length. This curvature determines the vibrational frequencies of the cluster. It is well known that SCF calculations systematically yield frequencies that are larger than the experimental ones. On the other hand, the X_α method systematically underestimates vibrational frequencies. In Sec. VI we will address this point further. Note that calculations that include correlation interaction (MP2 and SDCI) fall halfway between the SCF and X_α curves.

Since most of the quantum-chemical literature deals with geometries at, or very close to, equilibrium, it is difficult to judge the accuracy of either of the potential-energy curves far from equilibrium. Below, we will adopt the SCF surface as the standard potential-energy surface of the clusters. Occasionally, a comparison will be made with results that are obtained by using the X_α surface.

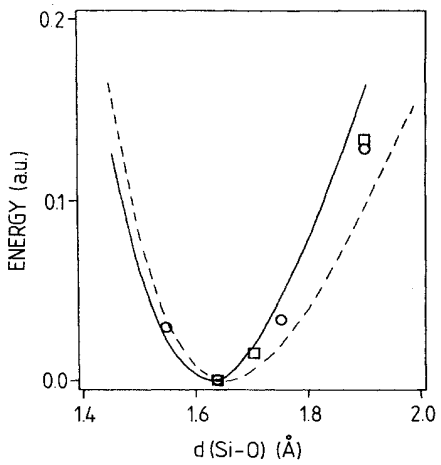

FIG. 3. Potential-energy surfaces of the T_d mode of H_4SiO_4, using the SCF-RHF (solid curve) and X_α methods (dashed curve). For a few Si-O distances, MP2 and SDCI corrections to the RHF-SCF results have been calculated (denoted by circles and squares, respectively).

III. PARAMETRIZATION OF THE POTENTIAL-ENERGY SURFACE OF CLUSTERS

The use of interatomic potentials for the calculations of static and dynamic properties of molecules, liquids, and solids is widespread. There are marked differences between the potential-energy functions used in different fields of application. In general, there seems to be a division between the chemical and the physical approach. The first, used in particular for the simulation of organic molecules, uses intricate force fields with a very large number of terms and parameters that are derived either from empirical data[18] or from *ab initio* calculations on small molecules.[19] Also, the energy functions are tied to the bonding scheme within the molecules. The approach commonly encountered in the physics literature uses force fields with fewer terms and fewer parameters (quite often determined empirically). The potential-energy functions are usually distance dependent and allow for changes in the local coordination of atoms.[20–22]

In line with previous work on silicates,[20] we adopt a simple two-body potential-energy function of the form

$$E^{2B}=\sum_{i>j}\frac{q_{\alpha_i}q_{\alpha_j}}{r_{ij}} + \sum_{i>j}\left[A_{\alpha_i\alpha_j}\exp(-b_{\alpha_i\alpha_j}r_{ij})-C_{\alpha_i\alpha_j}r_{ij}^{-6}\right] . \quad (1)$$

The first term contains the long-range electrostatic interaction between the effective charges on atoms i and j, dependent on their species (α_i,α_j). The second summation contains the short-range interactions that represent both the covalent bonding interaction between neighboring atoms (T-O) as well as the short-range repulsion between oxygen atoms, which stabilize the tetrahedral arrangement around the T atoms. $A_{\alpha\beta}$, $b_{\alpha\beta}$, and $C_{\alpha\beta}$ are parameters whose values depend on the interacting atom species α and β. The functional form is of the Buckingham type.

We emphasize at this point that the potential-energy functions are completely empirical. The fact that we use the same Si-O interaction for bonded and nonbonded atoms implies that no physical meaning can be attached to, e.g., the r^{-6} term (i.e., it is *not* the van der Waals interaction). Also, the parametrization given below can, in principle, be done again for a different functional form of the potential energy.[23]

Possible extensions of this potential-energy function are, e.g., the inclusion of a three-body bending term to stiffen the T-O tetrahedron,

$$E^{3B}=k_b(\theta-\theta_0)^2 , \quad (2)$$

where θ is the O(i)-T-O(j) bond angle and $\theta_0=109.47°$. Another example is the description of oxygen as a composite entity: a positive core, connected to a negatively charged, massless shell via

$$E^{\text{core-shell}}=k(\mathbf{r}_{\text{core}}-\mathbf{r}_{\text{shell}})^2 . \quad (3)$$

These particular extensions are used in the empirical shell-model force field of Catlow and co-workers,[24] with

which we will compare our results.

When a particular potential-energy function is chosen, the free parameters are optimized in such a way that the sum of the energy differences of all N cluster conformations that form the potential-energy surface is minimal:

$$\chi^2=\frac{1}{N}\sum_i^N (E_i^{\mathrm{SCF}}-E_i^{2B})^2 , \tag{4}$$

The final χ^2 values obtained are typically 5×10^{-7} or lower, corresponding to average discrepancies of the order of a millihartree.

The approach advocated here is to restrict the number of force-field terms and parameters to the minimum. The reason for this is that the more elaborate a parameter set becomes, the lower its transferability from one structure to the next will be. Modeling of SiO_2 requires (i) an effective silicon charge ($q_{Si}=-2q_O$), (ii) a Si-O, and (iii) an O-O short-range interaction. The latter enforces a tetrahedral arrangement of the oxygen atoms around the central silicon atoms. Hence a judicious choice of O-O parameters will make a three-body O-Si-O bending term superfluous. Likewise, the core-shell splitting, as used in the shell model [Eq. (3)], is not considered, since this mainly serves to screen charges, which can also be achieved by lowering q_{Si}. Also, in contrast to the force field of Tsuneyuki *et al.*, we do not explicitly include a Si-Si interaction other than the electrostatic interaction because the model cluster used to determine the potentials contains only a single silicon atom. The Si-Si interaction in the force field of Tsuneyuki *et al.* arises as a consequence of their parameter definition ($A_{\alpha\beta}=A_\alpha A_\beta$, $b_{\alpha\beta}=b_\alpha+b_\beta$, and $C_{\alpha\beta}=C_\alpha C_\beta$).

Even the determination of the seven remaining parameters is not unambiguous. This has been realized before, with respect to the charge "parameter." In previous attempts,[3-5] authors have always fixed the atomic charges beforehand. The remaining short-range parameters are determined by fitting the potential-energy function to the *ab initio* potential-energy surface. The rationalization for this duality in the parametrization lies in the infinite range of the Coulomb interaction, as a result of which one cannot reliably estimate its strength from the potential-energy surface of a small cluster.

Previously,[6] we have shown that a similar argument holds for some of the short-range parameters: the effective range of the Buckingham potential (especially between the oxygen atoms) is longer than the intracluster distances. This implies that also for some short-range parameters, gauging to bulk data is imperative in order to obtain reliable force fields. We will elaborate this point in Sec. IV.

IV. INCLUSION OF BULK INFORMATION

An unrestricted optimization of all parameters to fit the potential-energy surface of the H_4SiO_4 cluster is not feasible: convergence is obtained extremely slowly, if at

TABLE II. Force-field parameters.

	Short-range parameters			Charges
α_i-α_j	$A_{\alpha_i\alpha_j}$ (eV)	$b_{\alpha_i\alpha_j}$ (Å^{-1})	$C_{\alpha_i\alpha_j}$ (eV Å^6)	q_α
This work (SCF)				rigid ion
O-O	444.7686	2.485 13	0.0000	$q_O=-1.1$
Si-O	24 441.2370	4.935 04	180.8045	$q_{Si}=2.2$
This work (mixed SCF empirical)				rigid ion
O-O	1 388.7730	2.760 00	175.0000	$q_O=-1.2$
Si-O	18 003.7572	4.873 18	133.5381	$q_{Si}=2.4$
Al-O	16 008.5345	4.796 67	130.5659	$q_{Al}=1.4$
P-O	9 034.2080	5.190 98	19.8793	$q_P=3.4$
Na-O	3 542.2072	4.134 55	0.0000	$q_{Na}=1.0$
Na-Cl	5 783.1124	3.115 93	521.3348	$q_{Cl}=-1.0$
This work (X_α)				rigid ion
O-O	551.4486	2.900 00	0.0000	$q_O=-1.0$
Si-O	16 869.7220	4.862 58	124.9962	$q_{Si}=2.0$
Tsuneyuki *et al.* (Ref. 5)				rigid ion
O-O	1 753.8000	2.826 41	214.3700	$q_O=-1.2$
Si-O	10 703.0000	4.795 93	70.6100	$q_{Si}=2.4$
Si-Si	$8.615\,88\times10^8$	15.220 7	23.2603	
Catlow and co-workers (Ref. 24)				Shell model
O_s-O_s	22 764.0000	6.711 41	27.8800	$q_{O_s}=-2.869$
Si-O_s	1 283.9070	3.119 93	10.6615	$q_{Si}=4.0$
O_s-O_c	$k=74.92$ eV Å^{-2}			$q_{O_c}=0.869$
O_s-Si-O_s	$k=2.097\,24$ eV rad^{-2}, $\theta_0=109.47°$			

all, and parameters tend to adopt unphysical values (e.g., $C_{O\text{-}O} < 0$). Therefore we set $C_{O\text{-}O}$ equal to zero, implying no attractive oxygen-oxygen interaction. With this reduced parameter set convergence is much faster and minimum deviation is found for $q_{Si} = 2.2$, in reasonable agreement with the Mulliken value for the silicon charge (1.8, see Table I). We will refer to this force field as the SCF-force field, as it parametrizes the SCF potential-energy surface of H_4SiO_4. The parameters are listed in Table II. Note that our parameter values are remarkably close to the force-field parameters of Tsuneyuki *et al.*, given in Table II, even though these were derived from calculations on a different cluster.

With both force fields we have performed unrestrained lattice minimizations of the structure of α-quartz. A complete account of the lattice minimization algorithm used is given in Ref. 25. Remarkably, the force-field predictions for quartz, made with this force field, differ greatly from those obtained with the Tsuneyuki force field and are seriously at odds with experiment. The sharp disagreement with experiment is caused by the fact that the symmetry of our energy-minimized structure corresponds to that of β-quartz, the high-temperature phase of quartz.[26] In Sec. IV A the different phases of quartz will be discussed in more detail. The fact that apparently similar *ab initio* force-field yields make completely different predictions prompted us to study the connection between the potential-energy surface of a cluster and bulk systems in more detail.

The potential-energy surface of H_4SiO_4 is described by seven parameters. This is too large a number to determine all of them within physically acceptable regimes, i.e., values that do not cause unphysical behavior of the potential-energy functions at longer (*extra* cluster) distances. As an example, the D_{2h} mode potential-energy surface is determined primarily by the Coulomb repulsion of the oxygen atoms. The remaining difference is repulsive; once charges have been chosen it can be fitted accurately with an exponential function with $2\ \text{Å}^{-1} < b_{O\text{-}O} < 4\ \text{Å}^{-1}$. This implies that only one short-range parameter ($A_{O\text{-}O}$) can be determined from the potential-energy surface of the cluster. The situation is somewhat easier for the (bonded) Si-O interaction: once the O-O interaction is determined, the three short-range Si-O parameters are reliably determined from the T_d mode of the cluster. For convenience, we will call the parameters that are fitted to the *ab initio* data "cluster" parameters, to distinguish them from the "bulk" parameters, which are optimized in comparison with experimental results on a bulk system (quartz).

A. Phase diagram of quartz in parameter space

We will now explore the space spanned by the bulk parameters. For a series of points $(q_{Si}, b_{O\text{-}O}, C_{O\text{-}O})$ we have constructed the complete SiO_2 force field by fitting the cluster parameters to the SCF *ab initio* surface of H_4SiO_4. Subsequently, the results of unrestrained lattice minimizations of quartz made with these force fields were analyzed and compared with experimental data on quartz.

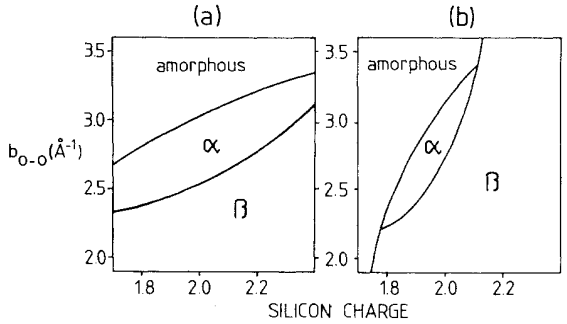

FIG. 4. Phase diagram of quartz in $(q_{Si}, b_{O\text{-}O})$ "bulk" parameter space ($C_{O\text{-}O} = 0$). Diagram (a) results if the remaining "cluster" parameters are fitted to the SCF-determined potential-energy surface of the H_4SiO_4 cluster; diagram (b) results if the X_α surface is used to fit the remaining parameters.

In Sec. III we pointed to the repulsive character of both the short-range and the long-range O-O interaction. This makes an attractive r^{-6} term superfluous at first sight. We will therefore set the bulk parameter $C_{O\text{-}O}$ equal to zero. This leaves us with a two-dimensional parameter space spanned by q_{Si} and $b_{O\text{-}O}$. For each point in bulk parameter space, we optimize the remaining cluster parameters to fit the *ab initio* potential-energy surface: $A_{O\text{-}O}$ is determined from the D_{2h} mode, the Si-O parameters from the T_d distortion mode. The relevant part of bulk parameter space is shown in Fig. 4(a), revealing three different symmetries of the energy-minimized structures: α-quartz, β-quartz, and an amorphous phase. For all calculations we started with the experimental structure of α-quartz.[12] The same picture emerges if the cluster parameters are fitted to the X_α potential-energy surface [Fig. 4(b)].

The different phases can easily be recognized from their structure and elastic properties. β-quartz, the high-temperature phase of quarts [$T > 846$ K (Ref. 26)], has the simplest structure, a hexagonal lattice (space group D_6^4) in which the silicon atoms reside on the symmetric positions $(\frac{1}{2}\frac{1}{2}\frac{1}{3})$, $(\frac{1}{2}00)$, and $(0\frac{1}{2}\frac{2}{3})$. As a consequence of the hexagonal structure, the C_{14} elastic constant equals zero.[27] α-quartz, the low-temperature phase of quartz, is trigonal with space group D_3^4. The silicon atoms occupy $(uu\frac{1}{3})$, $(u00)$, and $(0u\frac{2}{3})$, where u equals 0.4697 experimentally.[12] The amorphous phase, which in nature is easily formed from a silica gel or metal, is, in our calculations, earmarked by a triclinic unit cell (or rather simulation cell) with only trivial internal symmetry. The coordination of silicon by oxygen atoms is no longer strictly four (as for quartz): threefold and fivefold coordinations occur as well. Additionally, if calculations are performed with simulation cells containing two or four quartz unit cells, the translational symmetry within the simulation cell is lost during the minimization.

As mentioned in Ref. 6, the quality of the potential-energy function follows the SCF potential-energy surface to within 0.1 eV for all of the bulk parameter choices in

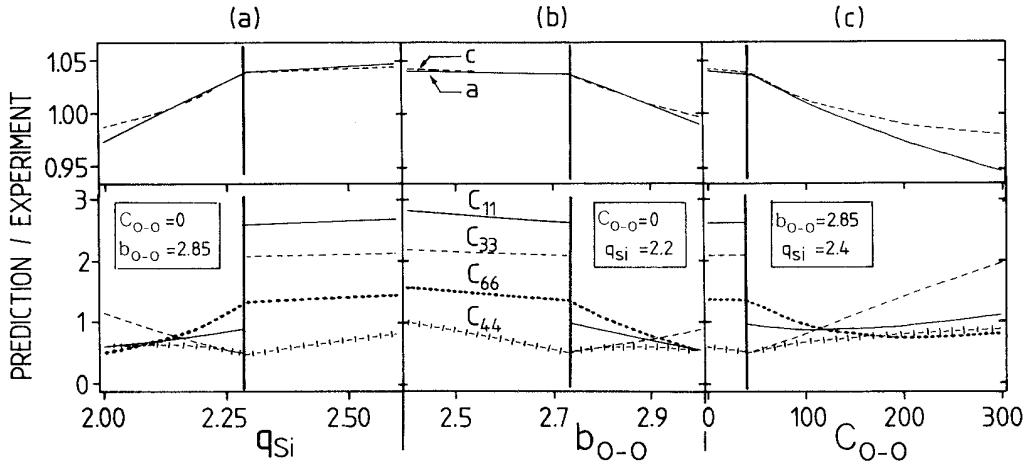

FIG. 5. Force-field predictions for the cell dimensions (upper curves) and elastic constants (lower curves), scaled to the experimental values for α-quartz vs "bulk" parameters (a) q_{Si}, (b) $b_{O\text{-}O}$ and (c) $c_{O\text{-}O}$. The thick solid lines indicate the α-β transition; the latter phase is characterized by extremely high values of C_{11} and C_{33}. Note that the curves for q_{Si} and $b_{O\text{-}O}$ are almost perfect mirror images of each other (taken from Ref. 6).

the range $1.9 < q_{Si} < 2.4$ and $2.4\ \text{Å}^{-1} < b_{O\text{-}O} < 3.0\ \text{Å}^{-1}$. The fact that the predictions for quartz with the various parameter sets differ so widely demonstrates the necessity to incorporate information about bulk systems into the force-field derivation.

B. Mixed *ab initio* empirical force field for quartz

The crystal symmetry of the energy-minimized structure can be considered to be binary information (true or false). The final mixing of the bulk parameters is done by comparing calculated unit-cell dimensions and elastic constants with experimental data on quartz. Although we will use experimental information on quartz in the subsequent force-field derivation, we want to emphasize that in principle the information on bulk systems can also be nonempirical. Such information may come, for example, from band-structure calculations on quartz. In recent years *ab initio* predictions of structure and compressibility of solids have become very accurate.[28,30]

The derivation of a force field for SiO_2 on the basis of both *ab initio* and bulk information is done by comparing the predictions for the unit-cell dimensions (a and c) and the diagonal elements of the elasticity tensor (C_{11}, C_{33}, C_{44}, and C_{66}) with experiment,[12,31] while varying the bulk parameters. We stress once again that for each combination of bulk parameters, the remaining cluster parameters are fitted to the *ab initio* potential-energy surface of the cluster.

Figure 5 shows scans of different bulk parameters. As seen from Figs. 5(a) and 5(b), the role of q_{Si} and $b_{O\text{-}O}$ is to some extent interchangeable: the variations of the unit-cell constants a and c and the elastic constants C_{ij} show similar patterns. Only when the restriction $C_{O\text{-}O}=0$ is lifted can good agreement with experiment be obtained. This implies that the parameter redundancy in the description of the cluster data (Sec. III) is removed in the description of the bulk data.

TABLE III. Comparison of force fields for α-quartz. Lengths are in angstroms; $d_{Si\text{-}O_1}$-$d_{Si\text{-}O_2}$ is the difference in the Si-O distance within a tetrahedron. The elastic constant (C_{ij}) are in 10^{10} N/m^2. The predictions closest to the experimental values are in boldface.

Obs.	Expt. (Refs. 12 and 31)	SCF	SCF empirical	Tsuneyuki	Catlow
a axis	4.913	5.113	**4.941**	5.018	4.837
c axis	5.405	5.613	**5.449**	5.548	5.347
u	0.4697	0.5000	**0.4648**	0.4602	0.4638
$d_{Si\text{-}O_1}$	1.614	1.609	1.605	1.6422	**1.615**
$d_{Si\text{-}O_2}$	1.605	1.609	1.597	1.6300	**1.608**
$d_{Si\text{-}O_1}$-$d_{Si\text{-}O_2}$	0.009	0.000	**0.008**	0.012	0.007
∠Si-O-Si	143.7	159.6	148.1	**146.8**	147.3
C_{11}	8.68	24.12	**9.05**	7.17	9.47
C_{33}	10.58	22.82	**10.70**	9.09	11.60
C_{44}	5.82	**5.16**	5.02	4.03	5.00
C_{66}	3.99	6.05	**4.12**	3.15	3.81
C_{12}	0.70	12.01	**0.81**	0.87	1.83
C_{13}	1.91	14.97	**1.52**	1.17	1.96
C_{14}	−1.80	0.00	**−1.76**	−1.43	−1.45

The final SCF empirical force-field parameters for SiO_2 are given in Table II. The predictions for α-quartz made with them are tabulated in Table III. In this table a comparison is made with predictions based on the previously mentioned SCF force field, the *ab initio* force field of Tsuneyuki *et al.*, and that of Catlow and co-workers. Note that the predictions of the SCF empirical approach are usually the best, also for properties which were not subject to the empirical fitting procedure such as the off-diagonal elements of the elasticity tensor and the coordinate of the silicon atoms u.

In Sec. V we will complement the comparison between the force fields with results on other SiO_2 polymorphs, but first we turn to the extension of the force field to include other four-coordinated framework elements.

C. Extension to other framework elements

As mentioned in the Introduction, important new classes of compounds are the aluminophosphates ($AlPO_4$, generally referred to as ALPO's) and silica-aluminophosphates. They were first synthesized by Flanigen and co-workers[32] and interest in them has risen especially since the discovery of VPI-5,[33] an ALPO with uniquely large, 12-Å pores. Hence a need has arisen for accurate Al-O and P-O potentials. *Ab initio* methods provide an ideal starting point for the derivation of such force fields. In this section we will derive these force fields and compare modeling results with experimental data on berlinite, the $AlPO_4$ analog of quartz.

We remind the reader that our aim is to derive a set of force-field parameters, which can be used concurrently, for instance when modeling a SAPO molecular sieve. Therefore we will assume that the O-O potential, which we derived above for use in the SiO_2 environment, also accounts for the O-O interaction in an $AlPO_4$ polymorph. This assumption immediately fixed the average of the aluminum and phosphorus charges at 2.4; the charge separation remains a free parameter, although, if we look ahead to the description of molecular sieves with a negative framework (compensated by positive cations such as Na^+), charge differences equal to the formal chemical charge differences are favored. For the moment we use dq as a free parameter, defined as

$$dq = q_{Si} - q_{Al} = q_P - q_{Si} = \tfrac{1}{2}(q_P - q_{Al}) \ . \tag{5}$$

Just as with the Si-O interaction, the parameters of the Al-O and P-O Buckingham potential can be determined unambiguously from the T_d distortion mode of the corresponding clusters. A check was made afterwards that the D_{2h} mode is accurately described by the O-O interaction previously determined for Si/O_2. Figure 6 shows the results of the force-field predictons for the unit-cell dimensions and elastic constants for berlinite as a function of the bulk parameter dq. At $dq \approx 0.55$, there is again a transformation between a β- and an α-phase. Just as with quartz, the experimental low-temperature phase is α-berlinite; at $T = 853$ K a structural phase transition to the hexagonal β-phase occurs.[34]

The comparison of a, c, and the diagonal elements of the elasticity tensor yields an optimal value of approximately 0.9 for dq. In view of the extendability of the parameter set to nonframework elements (see Sec. VII), we use the $dq = 1$ force field as the generic one. The parameters are tabulated in Table II. The final results for berlinite are given in Table IV. Note that the quality of the results is roughly the same as for quartz, even though the system is more complex. In Sec. V we will elaborate this point.

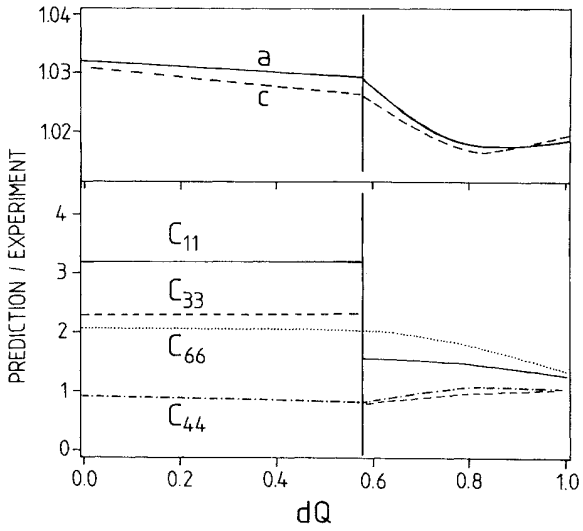

FIG. 6. Force-field predictions for the cell dimensions (upper curves) and elastic constants (lower curves), scaled to the experimental values for berlinite vs the "bulk" parameter dq. Note that as in Fig. 5, there is a clear symmetry change corresponding to the transition from β-berlinite to its α form.

V. TESTING OF THE FORCE FIELD

One of the questions that emerges from the above comparison of force-field predictions of quartz is whether or not the accuracy of the mixed *ab initio* empirical force field is maintained when applied to different SiO_2 polymorphs. Similarly, we want to know the reliability of

TABLE IV. Force-field predictions for berlinite. Units are the same as in Table III.

Obs.	Expt.	SCF empirical
a axis	4.943	5.050
c axis	10.948	11.169
u_{Al}	0.4664	0.4693
u_P	0.4669	0.4679
$d_{Al\text{-}O_1} - d_{Al\text{-}O_2}$	0.013	0.008
$d_{P\text{-}O_1} - d_{P\text{-}O_2}$	0.007	0.006
∠Al-O-P	142.9	150.7
	142.6	149.8
C_{11}	6.49	8.34
C_{33}	8.71	9.23
C_{44}	4.31	4.58
C_{66}	2.79	3.83
C_{12}	0.89	0.68
C_{13}	1.46	1.36
C_{14}	−1.21	−1.41

the $AlPO_4$ predictions.

With all four previously mentioned force fields, we have performed unrestrained lattice minimizations on three dense polymorphs of quartz (coesite, α-crystobalite, and the extremely dense stishovite, where silicon is six-coordinated by oxygen) and two microporous structures (zeolites) that exist as all-silica forms: silicalite (MFI) and sodalite. The results are shown in Table V. The overall picture that emerges from this comparison is that the accuracy of the SCF empirical force-field predictions is less for these systems than for quartz, which is obvious since a partial fit was made to the quartz data, but a marked improvement is seen with respect to the SCF force field. Also, the quality of the predictions is better than that obtained with the force fields of either Tsuneyuki or Catlow. This can be seen most clearly from Table VI, where the statistical accuracy of the predictions for both the lattice dimensions and the elastic properties is given.

From this we infer that by incorporating bulk data for one particular compound into the force-field derivation, the accuracy of force-field predictions on other polymorphs increases as well. This statement may be qualified by noting that the force-field predictions for stishovite have not benefited much from the calibration

TABLE V. Comparison of force fields for three dense and two microporous polymorphs of α-quartz. Symbols and units as in Table III. β is the angle between the a and the c axis; K is the bulk modulus.

Obs.	Expt.	SCF	SCF empirical	Tsuneyuki	Catlow
Coesite (Ref. 27)					
a axis	7.136	7.344	**7.138**	7.255	6.806
b axis	12.369	12.603	**12.493**	12.760	12.291
c axis	7.174	7.295	7.271	7.433	**7.115**
β	120.34	119.78	**120.76**	121.06	119.41
$\angle Si_1\text{-}O_1\text{-}Si_2$	180	**180**	**180**	**180**	**180**
$\langle \angle Si_1\text{-}O_x\text{-}Si_2 \rangle$	143.6	153.8	150.5	149.9	**146.5**
$\langle d_{Si_1\text{-}O} \rangle$	1.609	1.616	**1.604**	1.638	1.580
$\langle d_{Si_2\text{-}O} \rangle$	1.612	**1.613**	1.604	1.639	1.573
K	0.96	1.62	1.24	**1.00**	0.85
α-crystoballite (Ref. 48)					
a axis	4.978	5.255	4.920	5.001	**4.971**
c axis	6.948	7.432	6.602	6.718	**7.010**
$d_{Si\text{-}O_1}$	1.603	1.609	**1.608**	1.645	1.576
$d_{Si\text{-}O_2}$	1.610	**1.609**	1.595	1.628	1.575
$\angle$Si-O-Si	146.8	180.0	**143.9**	143.2	154.3
K		1.71	0.203	0.149	0.294
stishovite (Refs. 49 and 50)					
a axis	4.179	**4.161**	4.149	4.264	3.967
c axis	2.665	2.638	**2.662**	2.746	2.842
$d_{Si\text{-}O_1}$	1.809	**1.802**	1.790	1.836	1.750
$d_{Si\text{-}O_2}$	1.757	1.743	**1.755**	1.810	1.770
C_{11}	4.53	6.23	6.50	**5.08**	3.87
C_{33}	7.76	9.57	9.52	**7.13**	8.81
C_{44}	2.52	2.78	**2.75**	2.01	1.49
C_{66}	3.02	2.56	**2.72**	2.11	3.62
C_{12}	2.11	**2.24**	2.51	1.89	3.59
C_{13}	2.03	2.67	2.79	**2.26**	3.97
K	3.63	3.94	4.15	3.24	**3.71**
silicalite (Ref. 51)					
a axis	20.07	20.56	**20.37**	20.88	
b axis	19.92	20.45	**20.33**	20.81	
c axis	13.42	13.75	**13.68**	14.00	
$\langle \angle$Si-O-Si$\rangle$	168.3	155.9	162.2	**163.0**	
$\langle d_{Si\text{-}O} \rangle$	1.591	1.610	**1.606**	1.641	
K		1.04	0.284	0.290	
sodalite (Ref. 52)					
a axis	8.836	9.011	8.993	9.199	**8.768**

TABLE VI. Reliability of force-field predictions, as obtained from comparison of prediction with experiment for the five SiO_2 and the five $AlPO_4$ polymorphs mentioned in the text and mineral sodalite (SOD) and zeolite X. The numbers denote the average ratio between calculation and experiment and the spread therein.

	Obs.	SCF	SCF empirical	Tsuneyuki	Catlow
SiO_2	Cell dimensions	1.03±0.02	1.00±0.02	1.02±0.02	0.99±0.04
	Elastic moduli	1.31±0.66	1.10±0.18	0.88±0.17	1.18±0.51
$AlPO_4$	Cell dimensions		1.02±0.02		
	Elastic moduli		1.09±0.21		
SOD, X	Cell dimensions		1.00±0.01		
	Elastic moduli		1.4±0.3		

to the quartz data. Likely, the difference between four- and six-coordination of silicon is too large for sensible extrapolation. However, the fact that all *ab initio* force fields predict the structure and properties of stishovite fairly accurately, in spite of the fact that a four-coordinated cluster was used in the force-field derivation, is not as surprising as it may seem at first. In calculating the potential-energy surface of the cluster, we have stretched the Si—O bond to 2 Å and lowered the O-Si-O angle to 70°, well beyond the SiO distance and O-Si-O angle in stishovite.

All force-field testing was done at zero pressure. Recently, Chelikowski *et al.*[35] have compared the experimental pressure dependence of the structure of α-quartz, with force-field predictions made on the basis of Tsuneyuki's force field.[5] They conclude that some of the pressure-dependent properties are badly predicted due to inaccuracies in the modeling of the Si-O-Si bending in Tsuneyuki's potential. It would be interesting to learn the outcome of identical simulations with the force field proposed in this paper. The incorporation of (zero-pressure) data on α-quartz may have helped to determine the interaction between tetrahedrons more accurately, thereby lifting the cause of inconsistency observed by Chelikowski *et al.*

Table VII presents figures analogous to Table V for the microporous $AlPO_4$ polymorphs ALPO-5, -11, and -17,[1] and the newly synthesized 18-ring structure VPI-5.[33] Unfortunately, only structural information about these compounds is available, so the figure for the statistical accuracy of the elastic properties is based on berlinite data alone. Note that the accuracy of the SiO_2 predictions is basically preserved as we proceed to the more complex $AlPO_4$ systems.

TABLE VII. Force-field calculations for four $AlPO_4$ polymorphs. The meaning of the symbols and the units are the same as in Table III.

Obs.	Expt.	This work
ALPO-5 (Ref. 1)		
a axis	13.736	14.183
c axis	8.484	8.678
ALPO-11 (Ref. 1)		
a axis	13.5348	13.8456
b axis	18.4807	18.7746
c axis	8.3731	8.3847
ALPO-17 (Ref. 1)		
a axis	13.237	13.344
c axis	14.771	15.614
VPI-5 (Ref. 33)		
a axis	18.989	19.045
c axis	8.113	8.530

VI. VIBRATIONAL SPECTRUM OF α-QUARTZ

Vibrational spectra (infrared and Raman) of molecules and solids provide a good testing ground for both *ab initio* quantum-chemistry and for force-field methods. Therefore we conclude our discussion of the SiO_2 force fields by comparing their predictions for the vibrational, $k=0$ spectrum of α-quartz. Experimentally, both the frequencies and symmetry of the 24 optical vibrational modes are known,[36] enabling detailed comparison between theory and experiment.

Vibrational spectra, using the potentials of, respectively, the SCF empirical approach, the X_α surface, and those of the shell model (Table II), were calculated for wave vectors $(k00)$ and $(00k)$, with k equal to 0.001 reciprocal lattice unit. Reference 37 gives a full account of the factor group analysis for α-quartz. It suffices to say that the A_1 modes are Raman active, A_2 modes are infrared active, and E modes are both infrared and Raman active. The results are shown graphically in Fig. 7.

Using a Bethe lattice approach, van Santen and Vogel[38] have shown that the vibrational modes of four-coordinated SiO_2 polymorphs can be subdivided into three vibrational classes: (i) the highest frequencies (1100–1200 cm^{-1}) correspond to antisymmetric stretching of the Si—O bonds of the SiO_4 tetrahedron, (ii) the intermediate frequencies are due to a symmetric stretching of the Si—O bonds, while (iii) frequencies below approximately 550 cm^{-1} are due to bending in, and torsion between the tetrahedrons.

As the three classes each correspond to distinctly different modes of vibration of the SiO_4^{4-} cluster, it is instructive to compare the relative accuracies of the predictions for the three classes separately. The results of a modewise comparison of frequencies are given in Table VIII. Note that while the average discrepancy may be large (27%), the scatter is much lower ($\leq 7\%$), reflecting

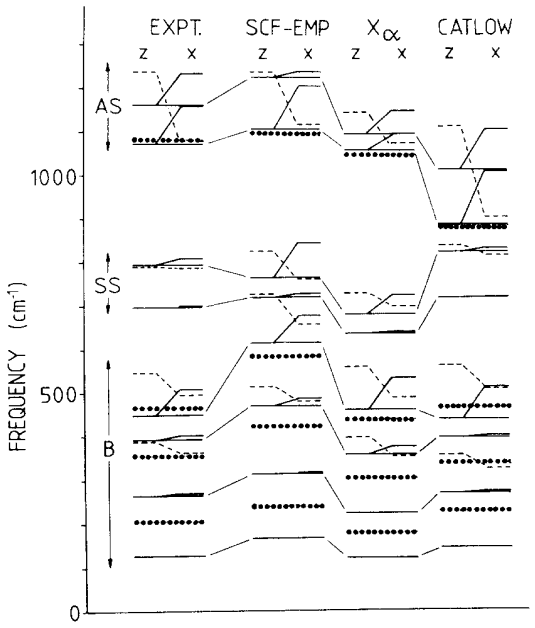

FIG. 7. Comparison between the experimental $k=0$ vibrational modes of α-quartz and the spectra as calculated with three different force fields (see Table II). B denotes bending modes; (a) SS and AS symmetric and antisymmetric stretching modes. Modes with symmetry label E (drawn lines) are degenerate for $k \| c$ (z in the figure) and split up into longitudinal and transversal modes for $k \perp c$ (denoted as x). A_2 modes are indicated by dashed lines, A_1 modes by dotted lines. The thin lines between corresponding E modes in different data sets serve as a guide to the eye.

the intercorrelation between the modes of one vibrational class.

The SCF empirical force field reproduces the values of the stretching modes better than the other force fields; the prediction of bending modes is notably worse. It is interesting to observe that this discrepancy is also present at the level of the *ab initio* calculations. We have calculated the harmonic vibrational frequencies of the SiO_4^{4-} ion at the same level as used for the calculation of the SCF potential-energy surface. A comparison with experimental data (Table VII) reveals the same discrepancies as for α-quartz.

An overall overestimation of vibrational frequencies by 10% is typical of SCF level calculations. At the same time, the X_α method underestimates frequencies by 5%.[39,40] This is precisely what is found in our predictions for α-quartz, based on the parametrization of the X_α potential-energy surface of H_4SiO_4.

Both these observations lead us to believe that the accuracy with which the vibrational spectrum of a bulk is predicted is directly related to the accuracy of *ab initio* cluster calculations. Note that the empirical force field by Catlow is quite accurate, but there is a difference in accuracy between the symmetric and antisymmetric stretching modes, which is absent for the force fields based on quantum-chemical data.

VII. NONFRAMEWORK ELEMENTS

Many interesting microporous structures (zeolites) contain aluminum atoms, which replace in part the silicon atoms of the framework. As the consequence of the formal charge difference between these atom types, the framework becomes negatively charged. This charge is compensated either by *extra*framework cations (Na^+, K^+, Ca^{2+}, etc.) or by acidic protons, attached to oxygen atoms that form a bridge between silicon and aluminum. Previous work on these systems was based on empirical potentials,[20] whose inadequacy became apparent in a study of Ooms *et al.*,[41] who could not find a minimized structure of zeolite X (faujasite with 1:1 Si-to-Al ratio). Here we present the first results on the inclusion of nonframework atoms into our *ab initio* force field.

Force-field parameters have been determined from the potential-energy surfaces of two clusters:

$$[H_4AlO_4]^- \cdots Na^+,$$

$$[H_4SiO_4] \cdots Na^+ .$$

The "zeolite" fragments are optimized structures, which

TABLE VIII. Statistical accuracy of the force-field predictions for the vibrational frequencies (infrared and Raman) of α-quartz. The mode assignment is taken from van Santen and Vogel (Ref. 38). Results for the harmonic vibrational frequencies of the SiO_4^{4-} ion, calculated in the RHF-SCF approximation, are given for comparison.

Mode(s)	Expt. (cm^{-1})	SCF empirical	X_α	Catlow
α-quartz				
antisymmetric stretch	1100–1200	1.03±0.02	0.96±0.03	0.86±0.03
symmetric stretch	700–800	1.02±0.04	0.90±0.02	1.03±0.01
bending	100–550	1.27±0.07	0.94±0.07	1.02±0.07
SiO_4^{4-} ion		SCF		
antisymmetric stretch	935	0.99		
symmetric stretch	775	1.05		
bending	460	1.29±0.13		
	275			

TABLE IX. Force-field calculations on systems with non-neutral frameworks: mineral sodalite. The meaning of the symbols and the units are the same as in Table III; K is the bulk modulus in Mbar.

Obs.	Expt.	This work
mineral sodalite	($Na_8Si_6Al_6O_{24}Cl_2$)	(Refs. 43 and 44)
a axis	8.870	8.79
$d_{Si\text{-}O}$	1.628	1.602
d_{Al-O}	1.728	1.738
∠Si-O-Al	138.3	136.1
$d_{Na\text{-}O}$	2.351	2.273
$d_{Na\text{-}Cl}$	2.730	2.784
C_{11}	8.8	11.4
C_{44}	3.6	3.9
C_{12}	3.9	6.7
K	0.55	0.82

the cation approaches in one of the O-T-O planes. The T-Na distance was varied between 2.0 and 4.4 Å. An additional calibration point is provided by fragments at infinite separation.[42] From the evaluation of the potential-energy curves at moderately large separation, as well as from the Mulliken charges, it is evident that the sodium ion has its full formal charge. An additional exponential repulsion term between oxygen and sodium is necessary to describe the interaction at shorter ranges. It appeared that the same short-range parameters (Table II) for the Na-O interaction adequately described the potential-energy surface of both clusters.

An interesting prototype of a sodium-loaded aluminosilicate is provided by mineral sodalite ($Na_8Si_6Al_6O_{24}Cl_2$) for which both structure and elastic properties are measured.[43,44] In this compound, the sodalite cage contains a Na_4Cl tetrahedron. As its modeling requires knowledge of the sodium-chlorine interaction, we have parametrized the Na-Cl interaction on the basis of SCF calculations on a NaCl pair (see Table II).

The results for the energy-minimized structure of mineral sodalite are given in Table IX. The structure in particular is accurately described. Table VI shows that the elastic properties are somewhat less accurately predicted than those for previously discussed compositions. Nevertheless, our approach yields a good description of compounds with this typical zeolite composition.

Complete localization of sodium ions in zeolite cages, as in mineral sodalite, is an exception rather than a rule. Most often, sodium ions are distributed more or less randomly in the zeolite cages, giving rise to crystallographic sites which are only partially occupied.[45] An example is provided by zeolite X ($Na_{96}Si_{96}Al_{96}O_{384}$), which has the faujasite structure. Its structure refinement[46] reveals sodium ion positions both fully and partially occupied. Part of the sodium ions could not be localized experimentally, and are supposedly distributed randomly over the faujasite cage.

This makes comparison with theoretical work not completely straightforward. Simulations are performed on a finite volume (one unit cell), extended via periodic boundary conditions. If we would occupy the partially occupied sodium sites randomly, translational symmetry will exaggerate the randomness relative to the experimental situation. Lattice minimizations performed with randomly sited sodium ions yielded distorted structures. The absence of symmetry in the cation siting caused a considerable break in the symmetry of the framework. This makes the results difficult to interpret and difficult to compare with experiment.

In order to avoid these problems, we have introduced fractional sodium ions, whose charge and repulsion parameter (A_{Na-O}) are reduced by the same number. Both the fractional occupation of the various sodium positions and the minimization results are given in Table X. The results obtained in this fashion are markedly better than those obtained starting from a random distribution of "full" sodium atoms over the crystallographic sites as

TABLE X. Force-field calculations on systems with non-neutral frameworks: zeolite X. The meaning of the symbols and the units are the same as in Table III. The fractional occupation of the various sodium ions in experiment (Ref. 46) and in the calculations is also indicated.

Obs.	Expt.	This work	Na^+	Filling factor expt.	Filling factor calc.
a axis	25.010	25.016			
$\langle d_{Si\text{-}O} \rangle$	1.62	1.60			
$\langle d_{Al\text{-}O} \rangle$	1.72	1.74			
⟨∠Si-O-Al⟩	141.4	139.6			
$d_{Na_1\text{-}O}$	2.43(×3)	2.34(×3)	Na_1	0.09	0.25
	3.13(×3)	3.19(×3)			
	3.24(×3)	3.38(×3)			
$d_{Na_2\text{-}O}$	2.35(×3)	2.25(×3)	Na_2	1.00	1.00
	2.88(×3)	3.08(×3)			
$d_{Na_3\text{-}O}$	2.30(×3)	2.21(×3)	Na_3	0.80	1.00
	2.94(×3)	3.09(×3)			
$d_{Na_4\text{-}O}$	2.29	2.19	Na_4	0.10	0.25
	2.80	2.83			
	2.90	3.38			

discussed above. This indicates the sensitivity of the zeolite framework for distortions caused by extra framework cations. The implication for zeolite modeling is that realistic modeling of zeolites (including extra framework ions) may require very large simulation cells.

VIII. CONCLUSION

We have outlined a route to develop effective interatomic force fields for zeolites from *ab initio* calculations on small clusters. It was shown explicitly that, while these calculations provide an excellent microscopic foundation of the short-range interactions, its full parametrization cannot be done without taking bulk properties into account. If bulk properties are taken into account, as we did by including experimental information on α-quartz, the quality of the predictions of the resulting force field is increased. Also, its transferability to other SiO_2 polymorphs is retained since this is guaranteed by the microscopic foundation of the force field.

It was shown that the SiO_2 force field could easily be extended to include additional elements (both intra- and extraframework) by parametrizing additional *ab initio* potential-energy surfaces. Although the number of parameters is thereby increased, the force-field accuracy remained the same, indicating the robustness of the present approach.

The relative ease with which extensions can be made makes this approach suitable for the modeling of complex state-of-the-art molecular sieves, such as SAPO's and possibly even the metal-substituted SAPO's.

[1]W. M. Meier and D. H. Olson, *Atlas of Zeolite Structure Types*, 2nd revised ed. (Butterworth, Cambridge, 1987).

[2]See, e.g., *Zeolites: Facts, Figures, Future*, Vol. 49 of *Studies in Surface Science and Catalysis*, edited by P. A. Jacobs and R. A. van Santen (Elsevier, Amsterdam, 1989).

[3]A. C. Lasaga and G. V. Gibbs, Phys. Chem. Miner. **14**, 107 (1987).

[4]A. C. Lasaga and G. V. Gibbs, Phys. Chem. Miner. **16**, 28 (1988).

[5]S. Tsuneyuki, M. Tsukada, H. Aoki, and Y. Matsui, Phys. Rev. Lett. **61**, 869 (1988).

[6]B. W. H. van Beest, G. J. Kramer, and R. A. Van Santen, Phys. Rev. Lett. **64**, 1955 (1990).

[7]J. Sauer, Chem. Rev. **89**, 199 (1989).

[8]The symmetry labels denote the symmetry of the central (distorted) tetrahedron. The terminal hydrogen atoms reduce the T_d and D_{2h} symmetries to S_4 and C_2, respectively.

[9]M. Dupuis, D. Sprangler, and D. Wendolowski, National Resource for Computation in Chemistry Software Catalog Program No. QG01, GAMESS Vol. 1 (1980); M. F. Guest and J. Kendrick, GAMESS User Manual, An Introductory Guide, CCP/86/1, Daresbury Laboratory, 1986.

[10]R. Poirier, R. Kari, and I. G. Csizmadia, *Handbook of Gaussian Basis Sets*, Vol. 24 of *Physical Sciences Data* (Elsevier, Amsterdam, 1985).

[11]J. C. Barthelat, P. H. Durand, and A. Serafina, Mol. Phys. **33**, 159 (1977).

[12]L. Levein, C. T. Prewitt, and D. J. Weidner, Am. Mineral. **65**, 920 (1980).

[13]D. Schwarzenbach, Z. Kristallogr. **123**, 161 (1966).

[14]A. Szabo and N. S. Ostlund, *Modern Quantum Chemistry: Introduction to Advanced Electronic Structure Theory* (MacMillan, New York, 1982).

[15]J. W. D. Connolly, *Modern Theoretical Chemistry* (Plenum, New York, 1977), Vol. 7.

[16]*Density Functional Theory*, Vol. 187 of *Lecture Notes in Physics*, edited by J. Keller and J. L. Gázquez (Springer-Verlag, Berlin, 1983).

[17]L. Hedin and B. I. Lundqvist, J. Phys. C **4**, 2064 (1971).

[18]N. L. Allinger, Y. H. Yuh, and J.-H. Lii, J. Am. Chem. Soc. **111**, 8551 (1989).

[19]J. Maple, U. Dinur, and A. T. Hagler, Proc. Natl. Acad. Sci. U.S.A **85**, 5350 (1988).

[20]See, e.g., R. A. Jackson and C. R. A. Catlow, Mol. Simulation **1**, 207 (1988).

[21]B. P. Feuston and S. H. Garofalini, J. Chem. Phys. **89**, 5818 (1988).

[22]J. Tersoff, Phys. Rev. Lett. **61**, 2879 (1988).

[23]We have tried the Lennard-Jones functional form. The results were not as good as those obtained for the Buckingham potential, which may be due to the fact that the Lennard-Jones potential contains fewer parameters.

[24]M. J. Sander, M. Leslie, and C. R. A. Catlow, J. Chem. Soc. Chem. Commun. 1271 (1984).

[25]C. R. A. Catlow and W. C. Mackrodt, in *Computer Simulation of Solids*, edited by C. R. A. Catlow and W. C. Mackrodt (Springer-Verlag, Berlin, 1982).

[26]J. D. Axe and G. Shirane, Phys. Rev. B **1**, 342 (1970).

[27]J. F. Nye, *Physical Properties of Crystals* (Oxford University Press, Oxford, 1985).

[28]S. G. Louie, *Electronic Structure, Dynamics and Quantum Structural Properties in Condensed Matter* (Plenum, New York, 1985), p. 335.

[29]R. Dovesi, C. Pisani, C. Roetti, and B. Silvi, J. Chem. Phys. **86**, 6967 (1987).

[30]D. C. Allan and M. P. Teter, Phys. Rev. Lett. **59**, 1136 (1987).

[31]H. J. McSkimin, P. Andreatch, and R. N. Thurston, J. Appl. Phys. **36**, 1624 (1965).

[32]S. T. Wilson, B. M. Lok, C. A. Messina, T. R. Cannan, and E. M. Flanigen, J. Am. Chem. Soc. **104**, 1146 (1982).

[33]M. E. Davis, C. Saldarriaga, C. Montes, J. Garces, and C. Crowder, Zeolites **8**, 362 (1988).

[34]H. Arnold, Z. Kristallogr. Kristallgeom. Kristallphys. Kristallchem. **121**, 145 (1965).

[35]J. R. Chelikowski, H. E. King, Jr., and J. Glinnemann, Phys. Rev. B **41**, 10 866 (1990).

[36]J. Etchepare, M. Merian, and P. J. Kaplan, Chem. Phys. **60**, 1873 (1974).

[37]A. J. M. de Man, B. W. H. van Beest, M. Leslie, and R. A. van Santen, J. Phys. Chem. **94**, 2524 (1990).

[38]R. A. van Santen and D. L. Vogel, Adv. Solid State Chem. **1**, 151 (1989).

[39]C. E. Dijkstra, *Ab-initio Calculation of Structures and Properties of Molecules*, Vol. 58 of *Studies in Physical and Theoretical Chemistry* (Elsevier, Amsterdam, 1988).

[40]L. Fan, L. Versluis, T. Ziegler, E. J. Baerends, and W.

Ravenek, Int. J. Quantum Chem. Symp. **22**, 173 (1988).
[41]G. Ooms, R. A. van Santen, C. J. J. den Ouden, R. A. Jackson, and R. C. A. Catlow, J. Phys. Chem. **92**, 4462 (1988).
[42]Such a calibration is not advisable for bonded interactions. Clearly, one is not interested in correctly predicting the dissociation energy of the H_4SiO_4 cluster.
[43]V. J. Löns and H. Schulz, Acta Crystallogr. **23**, 434 (1967).
[44]Z. Li, M. V. Nevitt, and S. Ghose, Appl. Phys. Lett. **55**, 1730 (1989).
[45]W. J. Mortier, *Compilation of Extra Framework Sites in Zeolites* (Butterworth, Guildford, 1982).
[46]Y. I. Smolin, Y. F. Shepelev, I. K. Butikova, and V. P. Petranovskii, Kristallografiya **28**, 72 (1983) [Sov. Phys.—Crystallogr. **28**, 36 (1983)].
[47]L. Levien and C. T. Prewitt, Am. Mineral. **66**, 324 (1981).
[48]D. P. Peacor, Z. Kristallogr. **138**, 274 (1973).
[49]W. H. Bauer and A. A. Khan, Acta Crystallogr. B **27**, 2133 (1971).
[50]M. E. Striefler and G. A. Barsch, J. Geophys. Res. **81**, 2453 (1976).
[51]D. H. Olson, G. T. Kokotailo, S. L. Lawson, and W. M. Meier, J. Phys. Chem. **85**, 2238 (1981).
[52]D. M. Bibby and M. P. Dale, Nature **317**, 157 (1985).